Astron. Astrophys. 207, 123–131 (1988)

ASTRONOMY AND ASTROPHYSICS

Radiation-driven winds of hot stars

V. Wind models for central stars of planetary nebulae

A. Pauldrach[1], J. Puls[1], R.P. Kudritzki[1], R.H. Méndez[1, 2, 4], and S.R. Heap[3]

[1] Institut für Astronomie und Astrophysik, Scheinerstr. 1, D-8000 München 80, Federal Republic of Germany
[2] Instituto de Astronomia y Fisica del Espacio, C.C. 67, 1428 Buenos Aires, Argentina
[3] Goddard Space Flight Center, Greenbelt MD 20771, USA
[4] Max-Planck-Institut für Astrophysik, Karl-Schwarzschild-Str. 1, D-8046 Garching bei München, Federal Republic of Germany

Received May 2, accepted May 21, 1988

Summary. Wind models using the recent improvements of radiation driven wind theory by Pauldrach et al. (1986) and Pauldrach (1987) are presented for central stars of planetary nebulae. The models are computed along evolutionary tracks evolving with different stellar mass from the Asymptotic Giant Branch. We show that the calculated terminal wind velocities are in agreement with the observations and allow in principle an independent determination of stellar masses and radii. The computed mass-loss rates are in qualitative agreement with the occurrence of spectroscopic stellar wind features as a function of stellar effective temperature and gravity.

Key words: stellar winds – central stars of planetary nebulae – mass – loss

1. Introduction

It is well established that stellar winds are a generic feature of young luminous stars with masses larger than 20 $M_\odot$, and that the evolution of these objects is strongly affected by severe mass loss connected with the stellar winds.

Until recently, the situation was less clear for the hot, low-mass stars in the advanced stage of post-AGB evolution – the central stars of planetary nebulae (CSPN). The advent of the IUE satellite permitted to confirm that in many CSPN supersonic stellar winds are present (Heap, 1979; Perinotto, 1983). However, there are also many CSPN that do not show stellar winds in their spectra. What is the reason for the difference?

The general situation was first described by Cerruti-Sola and Perinotto (1985). Their conclusion, which suffered somewhat from uncertainties in stellar luminosities and effective temperatures, was that the presence of a wind is a gravity effect (in their words, CSPN with smaller gravities almost always have winds, while at larger gravities the presence of a wind is less frequent).

This picture was partially modified by the results of a detailed, quantitative high-resolution spectroscopic study of CSPN by Méndez et al. (1988). They determined precise stellar effective temperatures and gravities, using non-LTE model atmosphere fits to the observed photospheric H and He absorption line profiles. Figure 1 shows their basic results concerning the stellar parameters, and also includes information about the presence of stellar winds.

Figure 1 shows that the decisive factor is not gravity alone, but luminosity – that is to say, the distance to the Eddington limit. Objects close to the Eddington limit show winds, and objects far from the Eddington limit do not show winds (which means that in this case the density or optical thickness of the surrounding wind plasma is not large enough to produce detectable emissions or absorptions in the spectra). This behaviour is in agreement with the idea that winds of CSPN are driven mainly by radiation pressure.

Another striking observational property of CSPN winds is the correlation of the terminal velocity v_∞ with $T_{\rm eff}$ (Heap, 1986; Pauldrach et al., 1988). We have spent some effort to reinvestigate this correlation carefully. We used only well exposed IUE high resolution spectra, which we reprocessed using a VAX-based IUE image processing system (Ahmad, 1987) at Goddard, allowing a good measurement of v_∞. In all cases the maximum value of outflow velocity inferred from the different wind lines in a single stellar spectrum was chosen. The values are generally accurate to $\pm 100\,{\rm km\,s^{-1}}$. This is confirmed by a comparison with the measurements quoted by Heap (1986) which normally agree within $100\,{\rm km\,s^{-1}}$. (Note that the new measurements on the improved reprocessed spectra have been performed independently in Munich). As for $T_{\rm eff}$, we have used the values determined by Méndez et al. (1988) for all IUE high-resolution objects in common with their sample. For the rest of the objects, we have derived $T_{\rm eff}$ using the available information about the hydrogen and helium II blackbody Zanstra temperatures (T_z(H) and T_z(He II)) and the nebular excitation classes. The procedure, which will be discussed in detail by Méndez et al. (1988, in preparation) uses the objects of Méndez et al. (1988) to establish correlations between (a) excitation class and spectroscopic $T_{\rm eff}$ (see Fig. 2) and (b) spectroscopic $T_{\rm eff}$ and blackbody Zanstra temperatures (see Fig. 3). We have derived our estimates of $T_{\rm eff}$ from these correlations.

Table 1 summarizes the results for two classes of CSPN: (a) objects of normal or roughly normal photospheric (He/H) ratio, and (b) extreme He stars, which do not show any trace of H in their photospheres (for a recent review on the latter objects, see

Send offprint requests to: R.P. Kudritzki

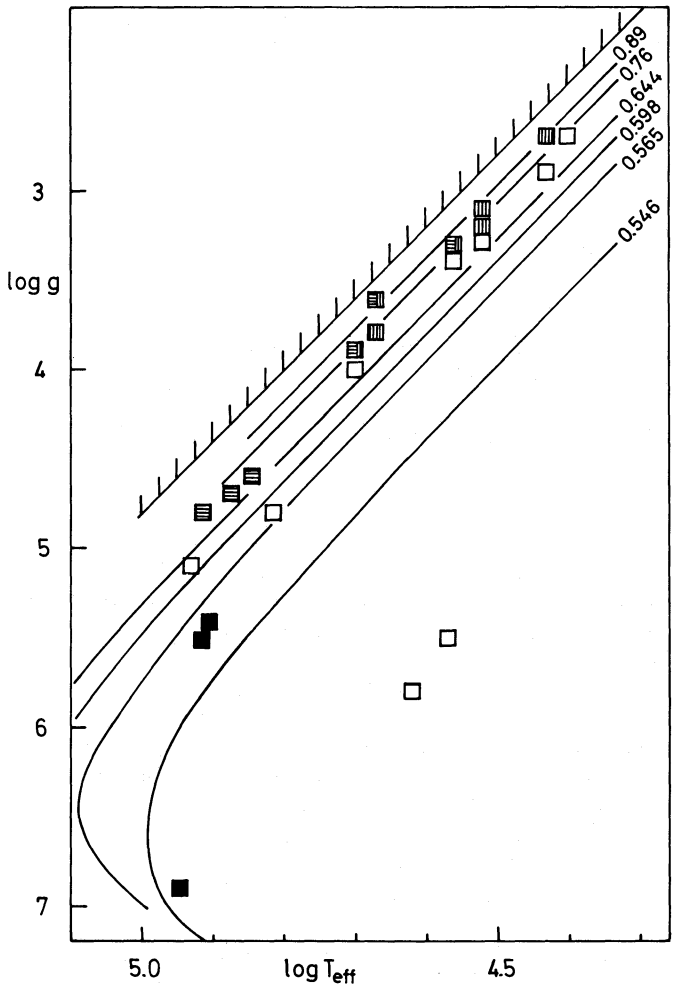

Fig. 1. The (log g, log $T_{\rm eff}$)-diagram of the CSPN analysed by Méndez et al. (1988). Evolutionary tracks evolving from the AGB towards hotter temperature (labeled by the stellar mass) are also shown. The individual CSPN are discriminated in the following way: ▤ winds detected by IUE; ▥ winds detected by optical emission lines (He II 4686, etc.); ■ definitely no winds neither in IUE nor optical; □ no winds in the optical, no IUE information available

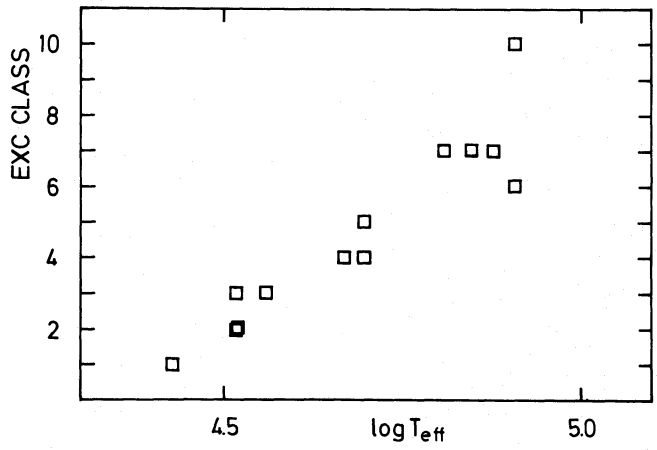

Fig. 2. The correlation of nebular excitation class with spectroscopic $T_{\rm eff}$ for the sample analysed by Méndez et al. (1988)

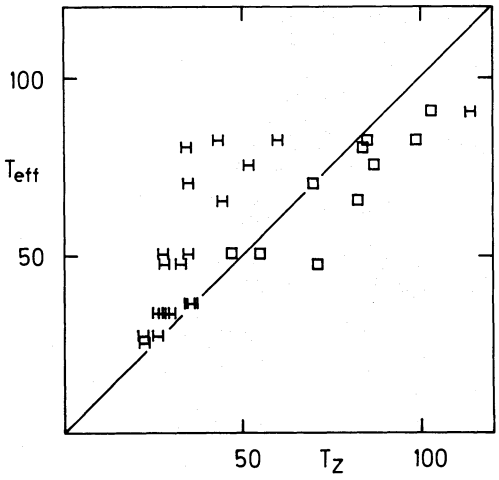

Fig. 3. Blackbody hydrogen Zanstra temperature (H) and He II Zanstra temperature (□) versus spectroscopic $T_{\rm eff}$ for the Méndez et al. (1988) sample. Note that only for the cooler objects $T_{\rm Z}$(H) lies near the diagonal line, whereas for hotter objects $T_{\rm Z}$(He II) is more reliable

Méndez et al., 1986a). Note that the value of $T_{\rm eff}$ for NGC 246 is the result of a detailed spectral analysis based on H-deficient non-LTE models (Husfeld, 1986).

Figure 4 demonstrates that v_∞ obviously increases with $T_{\rm eff}$. This behaviour is also consistent with the theory of radiatively driven winds. Since this theory predicts an increase of v_∞ with Vesc (the stellar surface escape velocity), a star moving along a constant-luminosity post-AGB evolutionary track towards higher $T_{\rm eff}$ is expected to show increasing v_∞, because meanwhile the stellar radius is decreasing.

Figures 1 and 4 provide then two strong, independent arguments supporting the idea that the winds of CSPN are radiation driven. This has encouraged us to undertake the calculation of a grid of wind models along post-AGB evolutionary tracks, in order to investigate how well can the theory of radiation driven winds reproduce the observed wind features of CSPN. In addition to the terminal velocities, v_∞, we will present, as a by-product of our calculations, also mass loss rates $\dot{M}$, which are of some importance for the evolutionary time scale of CSPN (Schönberner, 1983) and for the dynamical evolution of the surrounding nebula (Volk and Kwok, 1985; Schmidt-Voigt and Köppen, 1987a, b). These theoretical mass-loss rates might provide more useful information than the observed ones, as the latter are often highly uncertain (see Hamann et al., 1984, Perinotto, 1988).

2. Calculations

We have used the radiation driven wind code developed recently at Munich observatory (Pauldrach et al., 1986, hereinafter PPK). This code includes the finite cone angle effect of the incident photospheric radiation accelerating the wind. As has been demonstrated by PPK and Friend and Abbott (1986, hereinafter FA), this effect changes the wind dynamics significantly and leads to higher values of v_∞ and lower values of $\dot{M}$.

Table 2 gives the stellar parameters for our model grid. Note that the basic stellar parameter is the mass of the CSPN. According to the mass luminosity relation it yields the luminosity and then for different values of $T_{\rm eff}$ the stellar radius and gravity

Table 1. v_∞ and $T_{\rm eff}$ of CSPN

Object	Nebular excitation class (Refs. 8)	References for $T_{\rm eff}$ or T_Z	$T_{\rm eff}$ (10^3K)	v_∞ (km s^{-1})	Resonance line used
a) Normal hydrogen to helium ratio					
He 2-131		1, 2	30±5	750	C IV
IC 418	3	1	36±4	950	C IV
IC 4593	4	2, 3	40±10	1000	C IV
IC 2149	4	4	45±10	1200	C IV
NGC 2392	8p	1	47±7	600	N V
IC 3568	5	3	50±10	1800	N V
NGC 6826	5	4	50±10	1500	C IV
NGC 6210	5	2, 3	55±10	2300	N V
NGC 1535	7	1	70±7	2200	N V
NGC 3242	7	1	75±7	2200	N V
NGC 7009	6	1	82±10	2700	N V
b) Extreme helium-rich objects					
BD+30° 3639	1	5	30±5	950	Si IV
NGC 40	2	5	32±5	1600	C IV
NGC 6543	5	3	50±10	1800	C IV
Abell 30		6	100±30	3200	C IV
Abell 78		6	100±30	3400	C IV
NGC 246	10$^+$	7	130±15	>3300	C IV

References: 1. Méndez et al. (1988). 2. Freitas Pacheco et al. (1986). 3. Shaw (1985). 4. Heap (1977a, b). 5. Preite-Martinez and Pottasch (1983). 6. Kaler (1983). 7. Husfeld (1986). 8. Aller (1965), Heap (1975), Aller and Czyzak (1979)

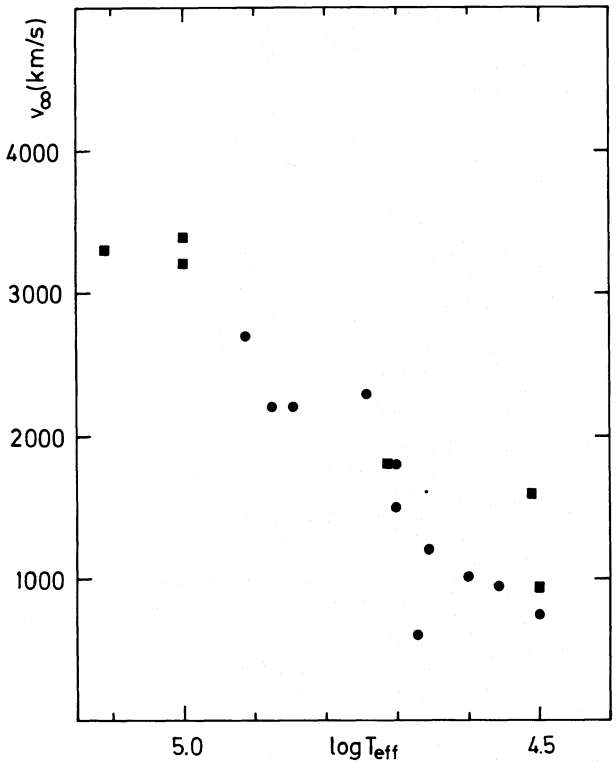

Fig. 4. The correlation of v_∞ with log $T_{\rm eff}$ for the objects of Table 1. Squares denote hydrogen deficient objects and circles describe objects with roughly normal hydrogen content

(note that for higher $T_{\rm eff}$ the slight decrease in luminosity along tracks of lower mass was taken into account). While after the work of Méndez et al. it appears reasonable that this core mass luminosity relation is applicable for CSPN with normal atmospheric hydrogen to helium ratio, it is an open question whether it holds for extreme helium rich CSPN. However, inspection of post giant stage evolution with helium burning shells only (Wood and Faulkner, 1986; Iben, 1984) yields mass luminosity relations, which are not too different. Thus for simplicity, we have used the same relation as for the objects with normal hydrogen content. The only difference between the normal and the H-deficient objects is then produced by Γ, the ratio of luminosity L to Eddington luminosity $L_{\rm E}$. This ratio enters in the formula for the escape velocity $v_{\rm esc}$,

$$v_{\rm esc}^2 = \frac{2GM_*}{R_*}(1-\Gamma). \qquad (1)$$

This happens because in the dynamical treatment of radiation driven winds we have to consider the radiative acceleration due to Thomson scattering.

Through Γ, $v_{\rm esc}$ depends on the (He/H) ratio for these hot stars.

Besides, Γ also affects the resulting mass-loss rate (see below).

For the treatment of the radiative line force in the hydrodynamic wind calculations the force multiplier parameters k, α, δ have to be specified (see PPK) by calculating the occupation numbers of all levels of all ions contributing. As the recent calculations by Pauldrach (1987) and Puls (1987) for the O4f star ζ Puppis have shown, this requires a detailed treatment of the

Table 2. Stellar parameters of the model grid. The second value for v_{esc} corresponds to extreme helium rich objects. The luminosities are taken from Schönberner (1983) and Wood and Faulkner (1986)

$M/M_\odot$	log $L/L_\odot$	T_{eff} (10^3 K)	log g (cgs)	v_{esc} (km s^{-1})	$M/M_\odot$	log $L/L_\odot$	T_{eff} (10^3 K)	log g (cgs)	v_{esc} (km s^{-1})
1.0	4.45	30	2.85	126	0.644	3.92	30	3.19	220
				187					239
		40	3.35	168			40	3.69	294
				250					320
		50	3.74	210			50	4.08	367
				313					401
		60	4.05	252			60	4.41	442
				371					490
		80	4.55	337			80	4.89	583
				494					642
		100	4.94	421			100	5.28	729
				621					806
0.565	3.55	30	3.50	285	0.546	3.08	30	3.96	392
				296					398
	3.54	40	4.01	383		3.08	40	4.45	523
				398					516
	3.54	50	4.40	479		3.06	50	4.91	677
				498					686
	3.53	60	4.72	575		3.04	60	5.20	799
				598					810
	3.51	80	5.24	780		3.00	80	5.75	1100
				809					1114
	3.47	100	5.68	1018					
				1051					

multilevel NLTE rate equations for all 133 ions including collisions and correct continuous radiative transfer. In principle we would have to repeat these calculations for each of the different stellar parameters in Table 2, which is of course an enormous effort. Instead, in the first step we have adopted the force multiplier parameters $k=0.053$, $\alpha=0.709$, $\delta=0.052$, obtained by Pauldrach (1987) for ζ Pup (see also Puls, 1987), for the whole grid of models, since we do not expect large differences from these values at least for $30000\,\mathrm{K} \leq T_{eff} \leq 50000\,\mathrm{K}$. We have subsequently justified this by calculating a few models in this temperature range for 0.65 $M_\odot$ and 1.0 $M_\odot$ with a selfconsistent determination of k, α, δ. For $T_{eff} \geq 50000$ K we encounter the problem that our line list (see Abbott, 1982; Kudritzki et al., 1987) becomes incomplete with respect to higher ionization stages. Thus, we would be able to calculate selfconsistent k, α, δ only by first completing the line list. This work is presently under way but still far from being finished. We therefore have no chance at the moment to check k, α, δ at higher temperatures. We are, however, convinced that the values adopted will at least allow a qualitative comparison with the observations.

3. Results

The results of our calculations with respect to v_∞ and $\dot{M}$ are summarized in Table 3. A graphical presentation as function of T_{eff} is given in Figs. 5 and 6. It is immediately seen that v_∞ in fact increases strongly with T_{eff} along an evolutionary track of constant luminosity. On the other hand $\dot{M}$ is mildly decreasing. This latter result is caused by the finite cone angle effect, since the old "radial streaming approximation" of the original theory by Castor et al. (1975, CAK) would yield constant $\dot{M}$ for constant k, α, L, M. The ratio of v_∞/v_{esc} is plotted in Fig. 7. The fact that this ratio varies between the different tracks and along them, although α is constant, is again caused by the presence of the finite cone angle correction factor (see PPK and FA). It is interesting to note that the fit formula $v_\infty/v_{esc}=\alpha/(1-\alpha)\times 2.21 \times (v_{esc}/1000\,\mathrm{km\,s^{-1}})^{0.2}$ as given by FA strongly disagrees with our results. The reason is that this formula neglects the influence of δ, the second force multiplier parameter, which reflects the change of the ionization structure in the wind. We will discuss the details of these finite cone angle effects in a separate paper, which will provide analytical solutions for the wind structure and formulae for v_∞ and $\dot{M}$ as a function of the stellar parameters. Here, we only demonstrate by Fig. 8 that v_∞/v_{esc} is obviously a function of v_s/v_{esc}, where v_s is the photospheric sound velocity.

The results of the few test calculations, which simultaneously solve the hydrodynamic equations and the rate equations for all 133 ions to provide the line force occupation numbers (for details see Pauldrach, 1987), are also given in Table 3 and Figs. 5 and 6. The effects for v_∞ are small, however for $\dot{M}$ larger differences are found in particular for the CSPN with 1 $M_\odot$, where $\dot{M}$ becomes significantly larger. The reason for this is that these objects are already very close to the Eddington limit. Since $\dot{M}$ is proportional to $(1-\Gamma)^{-1/\alpha}$ (see PPK or Kudritzki et al., 1988, in preparation), the wind becomes very dense in this case and the number of lines, which are able to contribute to the line force, increases. We,

Table 3a. Computed terminal velocities and mass loss rates, normal helium content

$M/M_\odot$	$T_{\rm eff}$ (10^3 K)	v_∞ (km s^{-1})	$\dot{M}$ ($10^{-6}\,M_\odot$/yr)	$M/M_\odot$	$T_{\rm eff}$ (10^3 K)	v_∞ (km s^{-1})	$\dot{M}$ ($10^{-6}\,M_\odot$/yr)
1.0	30	262	0.41	0.644	30	525	0.037
		240	1.18[a]			470	0.020[a]
	40	355	0.33		40	791	0.030
		400	1.52[a]			800	0.038[a]
	50	486	0.27		50	1074	0.027
		500	1.32[a]			910	0.046[a]
	60	586	0.26		60	1400	0.024
	80	852	0.21		80	1976	0.022
	100	1176	0.18		100	2614	0.020
0.565	30	815	0.0092	0.546	30	1318	0.0016
	40	1200	0.0076		40	1881	0.0014
	50	1598	0.0067		50	2583	0.0010
	60	2012	0.0060		60	3100	0.0010
	80	2931	0.0049		80	4505	0.00075
	100	4005	0.0037				

[a] Selfconsistent calculations with simultaneous new determination of k, α, δ

Table 3b. Computed terminal velocities and mass loss rates, extreme helium CSPN

$M/M_\odot$	$T_{\rm eff}$ (10^3 K)	v_∞ (km s^{-1})	$\dot{M}$ ($10^{-6}\,M_\odot$/yr)	$M/M_\odot$	$T_{\rm eff}$ (10^3 K)	v_∞ (km s^{-1})	$\dot{M}$ ($10^{-6}\,M_\odot$/yr)
1.0	30	541	0.13	0.644	30	781	0.019
	40	792	0.11		40	1120	0.017
	50	1054	0.10		50	1468	0.016
	60	1300	0.092		60	1870	0.014
	80	1836	0.080		80	2543	0.013
	100	2391	0.065		100	3268	0.012
0.565	30	1051	0.0057	0.546	30	1556	0.0010
	40	1498	0.0048		40	2109	0.0009
	50	1944	0.0043		50	2846	0.0007
	60	2381	0.0039		60	3428	0.0007
	80	3353	0.0033		80	4836	0.00053
	100	4468	0.0025				

therefore, conclude for the other grid points that v_∞ is described accurately enough by the ζ Pup force multiplier values k, α, δ, whereas $\dot{M}$ would differ by a factor of about two for $M<0.65\,M_\odot$ and would become larger up to a factor of five for $M>0.65\,M_\odot$, if completely selfconsistent calculations were performed.

4. A comparison with observations

Figure 1 indicates that winds are detected only in a limited domain of the (log g, log $T_{\rm eff}$)-diagram of CSPN. On the basis of our calculations we explain this by the change of wind density towards the Eddington limit. To demonstrate this is a simple way, we introduce the "mean wind line optical depth" $\bar{\tau}_{\rm w}$ as

$$\bar{\tau}_{\rm w}=10^8\,\frac{\dot{M}}{R_*\,v_\infty^2}, \qquad (2)$$

where $\dot{M}$ is given in $10^{-6}\,M_\odot$/yr, R_* in $R_\odot$ and v_∞ in km s^{-1}. The definition of $\tau_{\rm w}$ is motivated by the idea that in supersonically expanding winds the line optical depth $\tau_{\rm L}$ is proportional to $\rho(dv/dr)^{-1}$, which can be approximated roughly by $\bar{\rho}R_*/v_\infty$ and $\bar{\rho}=\dot{M}/(4\pi R_*^2\,v_\infty)$. The factor 10^8 is arbitrary, but would in principle correspond to a resonance line at 1200 Å with oscillator strength 0.1 of an element with 10^{-4} abundance relative to hydrogen, and an ionization stage which has an ionization fraction of 10^{-2}. Note that $\bar{\tau}_{\rm w}$ does not depend on temperature, which means that the $T_{\rm eff}$ dependence of the ionization fraction is not taken into account in this simple definition. Thus, we cannot expect that $\bar{\tau}_{\rm w}$ will describe the detectability of winds at very hot temperatures in a proper way. However, on the other hand $\bar{\tau}_{\rm w}$ is very suitable to demonstrate the increase of observable wind strength when approaching the Eddington limit. This is shown in Fig. 9, where the isocontours of log $\bar{\tau}_{\rm w}$ are plotted in the (log g, log

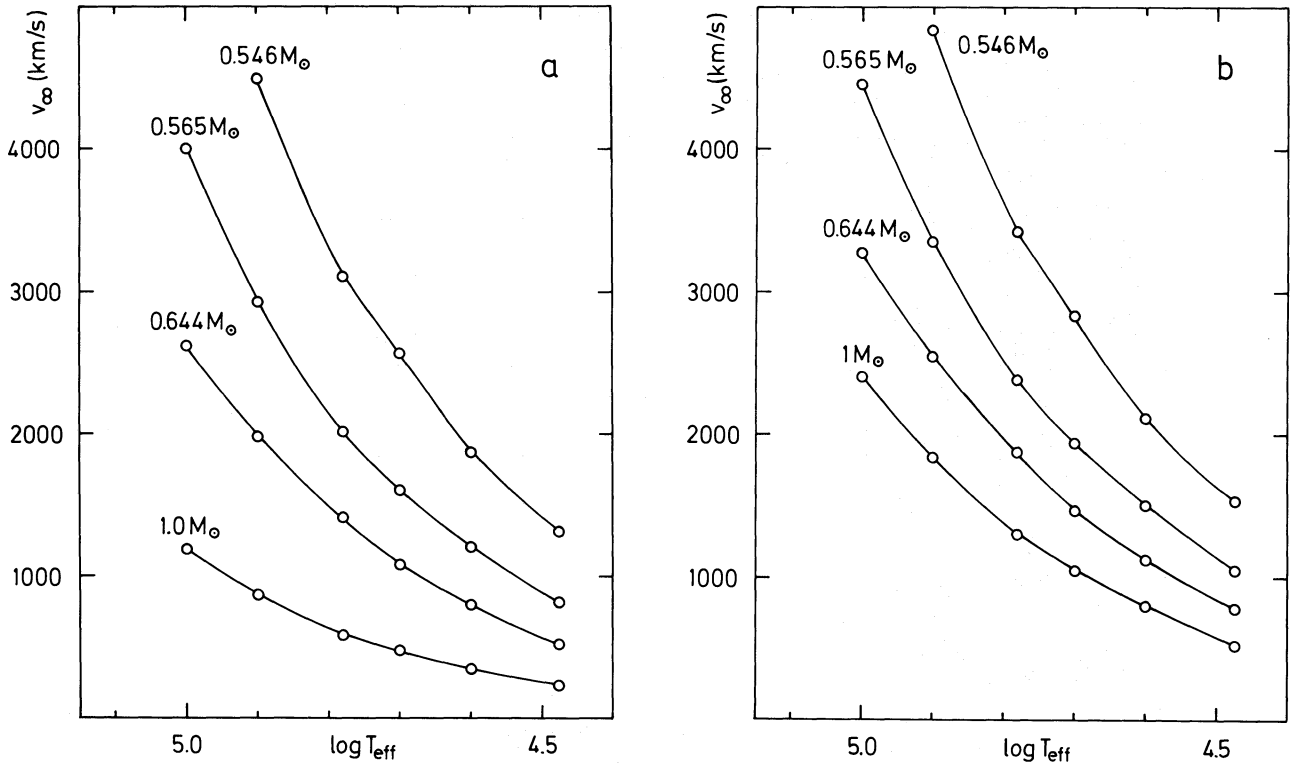

Fig. 5a and b. v_∞ as a function of $T_{\rm eff}$ calculated along evolutionary tracks labeled by their mass. **a** normal photospheric helium abundance, **b** Extreme helium photospheres

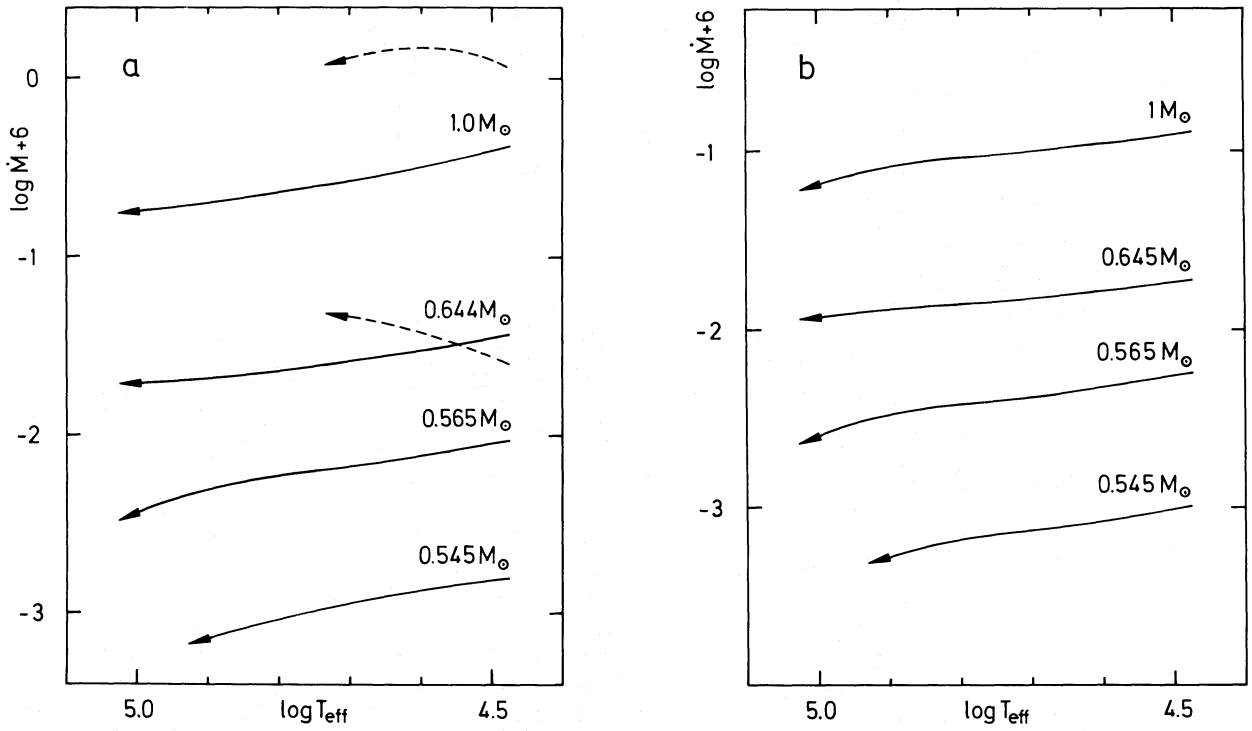

Fig. 6a and b. log $\dot{M}$ as a function of $T_{\rm eff}$. The dashed curves connect the results of fully selfconsistent calculations as described in the text

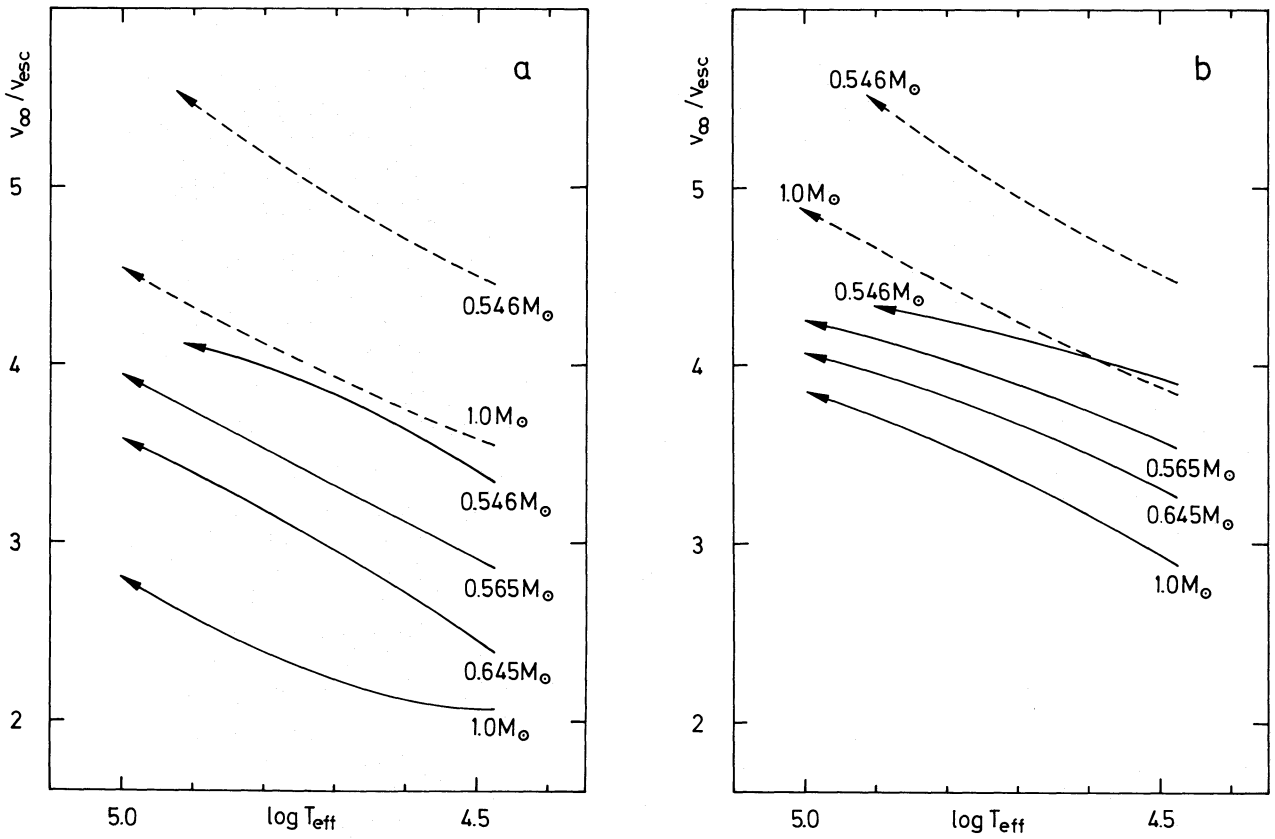

Fig. 7a and b. v_∞/v_{esc} as a function of T_{eff}. The dashed curves are examples of the scaling relation given by Friend and Abott (1986), which fails in this extreme case (see text)

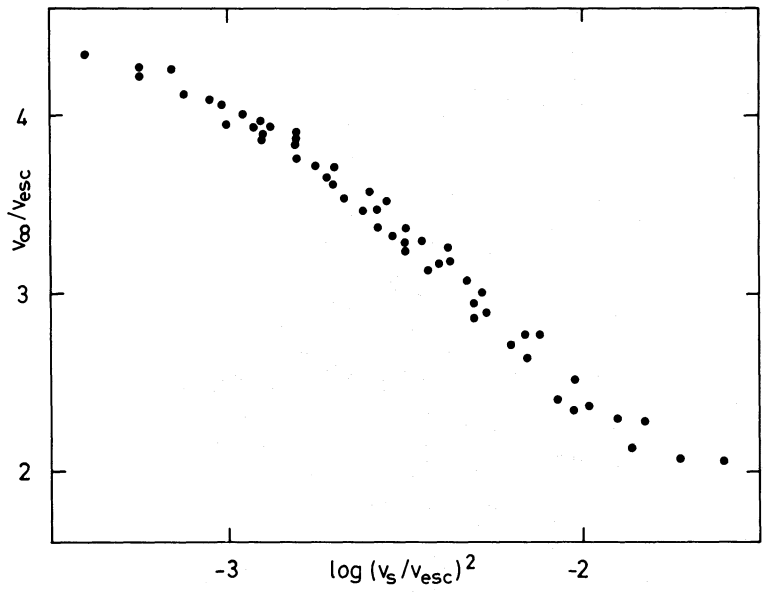

Fig. 8. v_∞/v_{esc} as a function of log $(v_s/v_{esc})^2$

T_{eff})-plane. Obviously, a change of 0.5 in log g can cause an increment of 100 in the wind optical depth, if the objects are close to the Eddington limit. This is in good qualitative agreement with Fig. 1. A more quantitative discussion based on calculated line profiles will be given in a separate paper (Gabler et al., 1988).

In Figs. 10 and 11 the observed v_∞ values are compared with the predictions of the radiation driven wind theory along the evolutionary tracks. The result is very encouraging, as the diagrams allow to read off an average mass of about 0.6 $M_\odot$, for our sample of CSPN. This just the canonical mass, which is

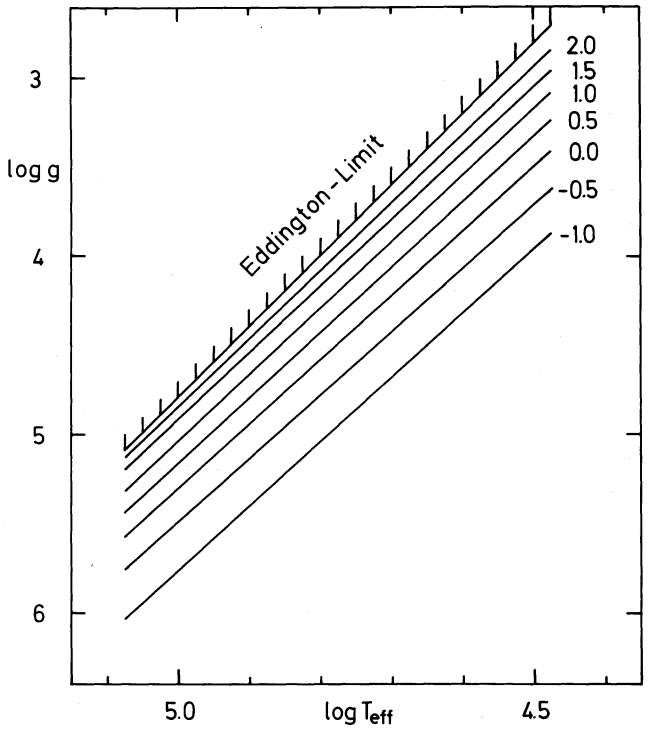

Fig. 9. Curves of constant logarithm of "mean wind line optical depth" $\bar{\tau}_w$ in the (log g, log T_{eff})-plane. (For a discussion, see text)

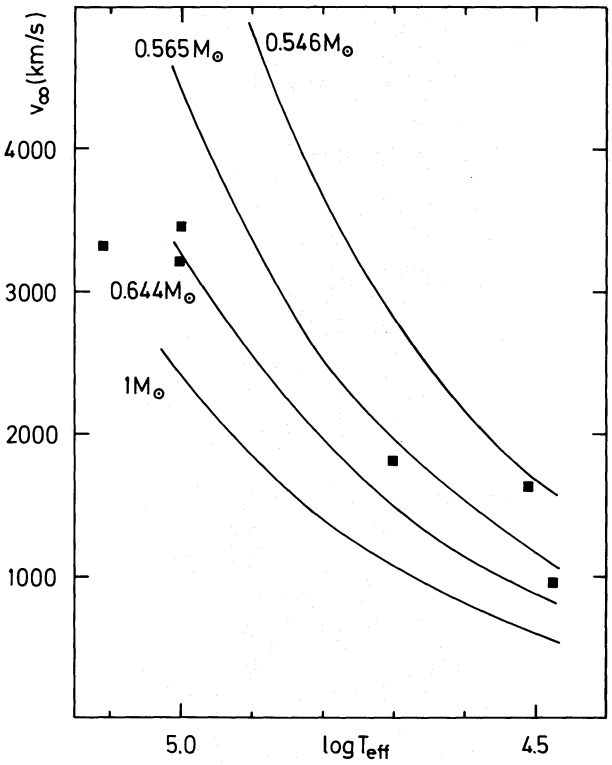

Fig. 11. Same as Fig. 10, but for extreme helium rich CSPN

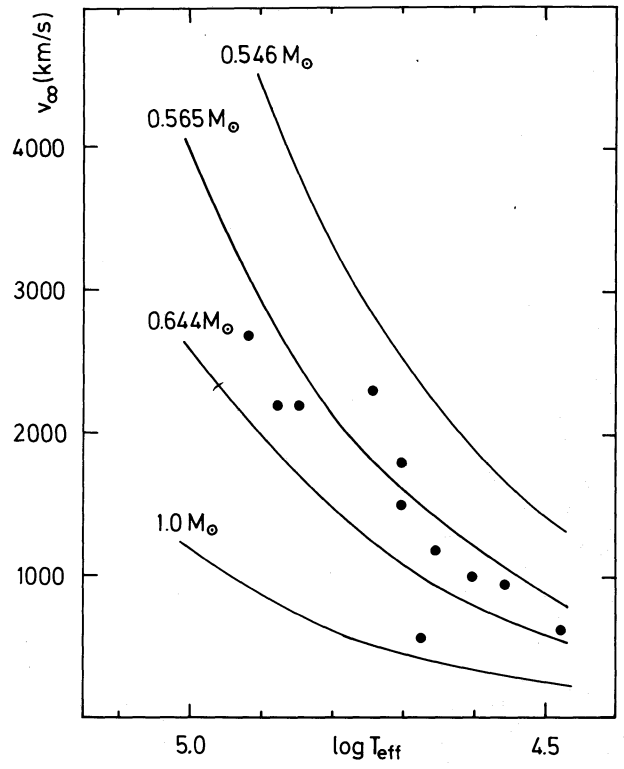

Fig. 10. v_∞ versus T_{eff} for CSPN of normal helium content compared with the wind calculations along the tracks

normally quoted for CSPN and DA White Dwarfs (Weidemann and Koester, 1984) and therefore indicates that radiation driven wind theory produces on the average the correct velocities. This is probably the only conclusion one should draw at the present stage of the theory. On the other hand, it is tempting to read off individual masses from the diagrams and to ask, whether these masses agree with the spectroscopic mass determination using the location of the stars in the (log g, log T_{eff})-plane and evolutionary tracks. This is done in Table 4, which shows that the masses generally agree within the error limits. An exception is IC 418, which however is a variable object with the characteristics of variable wind outflow (Méndez et al., 1986b). The "wind masses" of NGC 1535, 3242, 7009 appear to be systematically lower by 0.1 $M_\odot$. This could be caused by the fact that for these hot objects our fixed force multiplier parameters k, α, δ (see Sects. 2 and 3) are not accurate enough.

Anyhow, the present results are encouraging enough to investigate in future work the wind properties as an additional observational tool for constraining the evolutionary status of central stars. A quantitative analysis of stellar wind lines based on detailed selfconsistent wind models and computed line profiles, plus log g, log T_{eff} information from optical spectroscopy, appears to be a very attractive project.

Acknowledgements. This work was supported by the Deutsche Forschungsgemeinschaft under grant Ku 474-11/2. RHM would like to thank the Alexander von Humboldt Foundation (West Germany) for a research fellowship at the Institut für Astronomie und Astrophysik der Universität München, and the Max-Planck-Institut für Astrophysik (Garching) for additional support.

Table 4. Masses from v_∞ and quantitative spectroscopy

Object	$M/M_\odot$ from v_∞	$M/M_\odot$ from spectroscopy	Ref.
IC 418	$0.58\ ^{+0.1}_{-0.03}$	0.77 ± 0.07	1
NGC 2392	0.87 ± 0.15	0.90 ± 0.13	1
NGC 1535	$0.58\ ^{+0.07}_{-0.03}$	0.67 ± 0.04	1
NGC 3242	$0.60\ ^{+0.07}_{-0.05}$	0.68 ± 0.04	1
NGC 7009	$0.62\ ^{+0.07}_{-0.07}$	0.72 ± 0.06	1
NGC 246	$0.9\ ^{+0.1}_{-?}$	0.7 ± 0.2	2

References: (1) Méndez et al. (1988), (2) Husfeld (1986). The errors for the v_∞ masses are derived formally from the uncertainties of $T_{\rm eff}$ and v_∞. Note that v_∞ for NGC 246 is a lower limit

References

Abbott, D.C.: 1982, *Astrophys. J.* **259**, 282

Aller, L.H.: 1965, in Landolt-Börnstein, Group VI, Vol. 1, ed. H.H. Voigt, New York: Springer, p. 566

Aller, L.H., Czyzak, S.J.: 1979, *Astrophys. Space Sci.* **62**, 397

Ahmad, D.: 1987, DIPS Reference Manual

Castor, J.I., Abbott, D.C., Klein, R.I.: 1975, *Astrophys. J.* **195**, 157 (CAK)

Cerruti-Sola, M., Perinotto, M.: 1985, *Astrophys. J.* **291**, 237

Freitas Pacheco, J.A., Codina, S.J., Viadana, L.: 1986, MNRAS **220**, 107

Friend, D.B., Abbott, D.C.: 1986, *Astrophys. J.* **311**, 701 (FA)

Gabler, R., Wagner, A., Kudritzki, R.P., Pauldrach, A., Puls, J.: 1988, *Astron. Astrophys.* (in press)

Hamann, W.R., Kudritzki, R.P., Méndez, R.H., Pottasch, S.R.: 1984, *Astron. Astrophys.* **139**, 459

Heap, S.R.: 1975, *Astrophys. J.* **196**, 195

Heap, S.R.: 1977a, *Astrophys. J.* **215**, 609

Heap, S.R.: 1977b, *Astrophys. J.* **215**, 864

Heap, S.R.: 1979, in *IAU Symp.* **83**, p. 99

Heap, S.R.: 1986, in *Eighth Years of IUE*, Proc. Joint NASA/ESA/SERC Conference, ESA SP-263, p. 291

Husfeld, D.: 1986, Ph.D. Thesis, Universität München

Iben, I.: 1984, *Astrophys. J.* **277**, 233

Kaler, J.B.: 1983, *Astrophys. J.* **271**, 188

Kudritzki, R.P., Pauldrach, A., Puls, J.: 1987, *Astron. Astrophys.* **173**, 293

Méndez, R.H., Forte, J.C., Lopez, R.H.: 1986b, *Rev. Mex. Astron. Astrofis.* **13**, 119

Méndez, R.H., Kudritzki, R.P., Herrero, A., Husfeld, D., Groth, H.G.: 1988, *Astron. Astrophys.* **190**, 113

Méndez, R.H., Miguel, C.H., Heber, U., Kudritzki, R.P.: 1986a, in *Hydrogen Deficient Stars and Related Objects*, IAU Coll. 87, eds. K. Hunger et al., Reidel, Astrophys. Space Sci. Library **128**, p. 323

Pauldrach, A.: 1987, *Astron. Astrophys.* **183**, 295

Pauldrach, A., Puls, J., Kudritzki, R.P.: 1986, *Astron. Astrophys.* **164**, 86 (PPK)

Pauldrach, A., Kudritzki, R.P., Gabler, R., Wagner, A.: 1988, Proc. 2nd Torino Workshop *Winds from Stars and Active Galactic Nuclei*, eds. L. Bianchi, R. Gilmozzi, p. 63

Perinotto, M.: 1983, in *IAU Symp.* **103**, p. 323

Perinotto, M.: 1988, *Planetary Nebulae*, Proc. IAU Symp. 131 ed. S. Torres-Peimbert, invited paper (in press)

Preite-Martinez, A., Pottasch, S.R.: 1983, *Astron. Astrophys.* **126**, 31

Puls, J. 1987, *Astron. Astrophys.* **184**, 227

Schmidt-Voigt, M., Köppen, J.: 1987a, *Astron. Astrophys.* **174**, 211

Schmidt-Voigt, M., Köppen, J.: 1987b, *Astron. Astrophys.* **174**, 223

Schönberner, D.: 1983, *Astrophys. J.* **272**, 708

Shaw, R.A.: 1985, Ph.D. Thesis, Univ. of Illinois

Volk, M., Knok, S.: 1985, *Astron. Astrophys.* **153**, 79

Weidemann, V., Koester, D.: 1984, *Astron. Astrophys.* **132**, 195

Wood, P.R., Faulkner, D.J.: 1986, *Astrophys. J.* **307**, 659